ΠΑΝΕΠΙΣΤΗΜΙΟ ΚΡΗΤΗΣ
UNIVERSITY OF CRETE

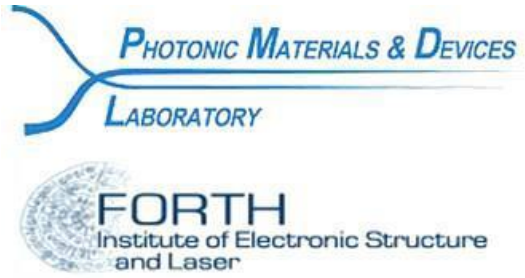

Whispering Gallery mode Resonation in Ion-Exchanged Borosilicate Glass Fibers

Thesis by

Kokkinidis Nikolaos

Supervisor: Dr. Pissadakis Stavros

2023

Acknowledgements

I would like to express my deepest appreciation to Dr. Pissadakis for his continuous support, and invaluable patience. His immense knowledge and plentiful experience have encouraged me in all the time. I would like to thank you very much for your support and understanding over the past year.

I would like to extend my sincere thanks to Dr. Korakas who guided, impacted and inspired me.

Lastly, I would be remiss in not mentioning my family, especially my parents. Their belief in me has kept my spirits and motivation high during this process.

Abstract

In the present thesis is presented an analysis on the potassium (K^+) ion-exchange process in borosilicate glass, optical fiber whispering gallery mode cavities. The ion-exchange was achieved using the melt bath technique in a potassium nitrate melt, for typical times of 11, 22 and 44 hours. With the help of a tapered optical fiber coupler, whispering gallery mode spectra were obtained, while by applying longitudinal strain on the cavity, the relevant mode shifting effects emerge, as well as the impact of the ion-exchange process on the photoelastic properties of the glass cavity material. To gain a better insight, energy-dispersive X-ray spectroscopy revealed the concentrations profiles of the potassium and sodium ions in different depths from the cavity's circumference, COMSOL Multiphysics simulations provided a valid digital representation of the system, and to investigate the effect of non-symmetrical ion-migration and corresponding refractive index annular changes, ion-exchanged cavities we thermally poled. Lastly, in order to study the Young's modulus modifications introduced by the ion-exchange process, the hardness Knoop was measured using the micro-indentation method on typical BK-7 slabs that had undergone the same treatment.

Contents

Glossary of Acronyms

WGM Whispering Gallery Mode

WGR Whispering Gallery Resonator

UHQ Ultra-high Quality factor

TE Transverse Electric

TM Transverse Magnetic

FSR Free Spectral Range

OSA Optical Spectrum Analyzer

SEM Scanning Electron Microscopy

EDX Energy-Dispersive X-ray spectroscopy

SMF Single-Mode optical Fiber

EDFA Erbium-Doped Fiber Amplifier

OFT Optical Fiber Taper

PMOF Polarizing-Maintaining Optical Fiber

1 Introduction

1.1 History of Whispering Gallery Resonators

In round structures, it was noticed that whispers or low murmurs were audible all around the circumference. This drew the attention of Lord Rayleigh who studied the phenomenon at the whispering gallery of St. Paul's Cathedral (1877) [1], [2]. The Cathedral's dome had such acoustic properties and it was soon realized that whispering gallery waves exist also for light waves.

In the same period, the works of Peter Debye [3] and Gustav Mie [4] helped with determining the equations for the resonant eigenfrequencies of free dielectric and metallic spheres, which also apply to Whispering Gallery Resonators. This was the starting point of the later developed wave theory concerning the whispering gallery resonators.

1.2 Applications of Whispering Gallery Resonators

Today the Whispering Gallery Resonators draw a lot of attention due to their unique combination of high-quality factors, low mode volumes, and small size. Another important trait is their ability to use the larger portion of the electromagnetic spectrum, from radio waves to X-rays, giving them a great variety of uses. Some notable applications are the development of photonic devices for sensing [5], lasing [6], and spectroscopic applications [7].

1.3 Wave theory of Whispering Gallery Modes

The theory concerning this thesis could be summarized by investigating scalar (e.g., acoustic waves or single components of the EM field) WGMs in a 2D cylindrical cavity of radius α. Starting from the wave equation, the refractive index difference between inside ($r < a$) and outside ($r > a$) the cavity results in two separate 2D Helmholtz equations:

$$\Delta^2\psi_\zeta + {k_{1,\zeta}}^2\psi_\zeta = 0 \quad , \quad r < a \quad and \quad \Delta^2\psi_\zeta + {k_{0,\zeta}}^2\psi_\zeta = 0 \quad , \quad r > a \qquad (1)$$

where $k_{0,1,\zeta} = {\omega_\zeta}/{c_{0,1}}$ is the wavenumber, ω_ζ are the resonant angular frequencies, $c_{0,1}$ is the refractive index outside (0) or inside (1) the cavity and $\psi_\zeta(\vec{r})$ are the eigenfunctions. The boundary conditions are: the function $\psi_\zeta(\vec{r})$ should be finite everywhere, it should describe only outgoing waves for $r \to \infty$ and it should be continuous at the edge of the cavity ($r = a$). By

applying these conditions, by separating the variables in a cylindrical coordinate system (r,φ) and by using the Bessel J_m and Hankel $H_m^{(1)}$ functions of the first order of m we obtain:

$$\psi_\zeta(\vec{r}) = e^{im\varphi} \cdot \begin{cases} A_\zeta J_{|m|}(nk_{0,\zeta}r) & ; \quad r < a \\ B_\zeta H_{|m|}^{(1)}(k_{0,\zeta}r) & ; \quad r > a \end{cases} \qquad (m \in \mathbb{Z}) \tag{2}$$

The boundary conditions give the B_ζ over A_ζ ratio and the characteristic equation which determines the eigenfrequency ω_ζ:

$$\frac{B_\zeta}{A_\zeta} = \frac{J_{|m|}(nk_{0,\zeta}a)}{H_{|m|}^{(1)}(k_{0,\zeta}a)} \quad ; \quad \frac{J_{|m|}'(nk_{0,\zeta}a)}{J_{|m|}(nk_{0,\zeta}a)} = \frac{1}{n}\frac{H_{|m|}^{(1)\prime}(k_{0,\zeta}a)}{H_{|m|}^{(1)}(k_{0,\zeta}a)} \tag{3}$$

Here, the prime denotes ordinary differentiation, and due to linearity, the actual values of A_ζ and B_ζ remain undetermined. The characteristic equation is transcendental and can only be solved numerically.

The eigenmodes and eigenfrequencies (the spectrum) depend on the optogeometric and dielectric parameters of the cavity. The light wave is propagated over the carved surface of the cavity by total internal reflection which is inherently imperfect leading to a degree of radial loss (Imω_ζ), also known as tunneling ray attenuation.

1.4 Evanescent coupling using tapered Optical fibers

The most efficient coupling today is achieved with tapered optical fiber couplers having efficiency that reaches 99.99%, for coupling fused silica resonators. The power transfer from tapered optical fiber to cavity resonator depends on the special overlap and phase matching of the effective refractive index.

The tapered optical fiber is single-mode and fabricated with a diameter of typically few micrometers for near-infrared wavelength. The fiber taper was placed vertical to the resonator perimeter allowing the entrance and exit of the output beam.

One downside of the tapered fibers is that they are quite fragile and effective only with cavity resonators with a refractive index comparable to silica (1.4-1.45).

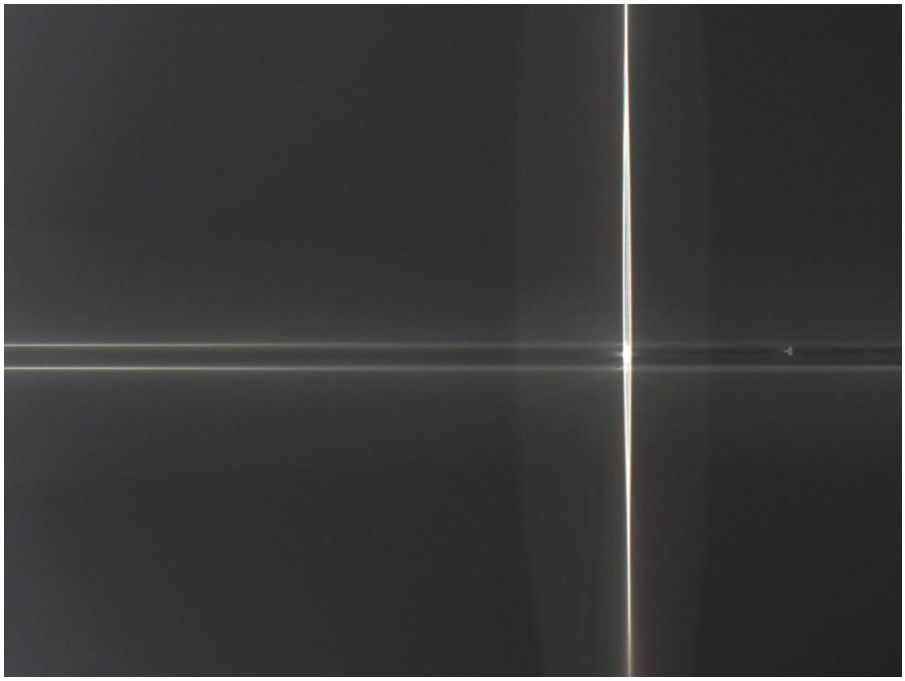

Figure 1.1: Photograph of the tapered optical fiber (vertical line) coupled to an optical fiber cavity (horizontal line).

1.5 Resonator parameters

The Quality factor (Q factor) of an optical resonator concerns the lifespan of the electromagnetic wave trapped within. Whispering gallery resonators usually have high Q factors allowing them to have quite high levels of sensitivity. The Q factor of a whispering gallery mode can be defined as:

$$Q = \omega_0 \frac{Stored\ energy}{Power\ loss} = \omega_0 \tau = \frac{\omega_0}{\Delta\omega_{FWHM}} \tag{4}$$

where $\omega_0 = 2\pi v_0$ is the angular frequency and v_0 is the frequency of the resonance, τ is the cavity ring down lifetime and $\Delta\omega_{FWHM}$ is the linewidth or the "uncertainty" of the frequency of the resonance (full-width-at-half-maximum or FWHM of the resonance peak) in angular frequency.

The Free Spectral Range (FSR) is the spectral range between two consecutive whispering gallery modes of the same radial order. It is given by:

$$FSR = \frac{\lambda^2}{2\pi n a} \tag{5}$$

where λ is the wavelength of the electromagnetic wave, n the refractive index and α the radius of the cavity.

1.6 Thesis outline

The aim of this thesis is the investigation of the potassium ion-exchange process in borosilicate glass, optical fiber whispering gallery mode cavities along with the effects it has on the photoelastic properties of the glass cavity material.

At first, specifications of the borosilicate glass optical fiber will be presented, followed by the apparatuses and processes utilized that list as follow: the potassium ion-exchange treatment using the melt bath technique applied for typical times of 11, 22 and 44 hours, fabrication of the tapered optical fibers by applying the heat and pull method, the spectral characterization for whispering gallery modes cavities apparatus for obtaining the respective spectra with a wavelength range between 1540 nm and 1560 nm, longitudinal strain application on the fiber cavities using a specialty made actuation fork and finally the thermal poling apparatus consisting of a twofold structure, made from stainless steel, that acted as non-conducting electrode configuration.

Moving to the experimental part of this thesis, whispering gallery mode spectra of pristine and potassium ion-exchanged borosilicate glass optical cavities will be presented. Obtaining from the spectra the free spectral range (FSR) between two consecutive fundamental (1^{st}) radial order modes, we estimated the refractive index changes in the ion-exchanged layer of the fiber cavities. Potassium and sodium ions concentrations profiles in different depths from the cavity's circumference are obtained using energy-dispersive X-ray spectroscopy. Additionally, using the COMSOL Multiphysics package and making use of the Wave Optics, Electromagnetic Waves, Frequency Domain, simulations reveal the distribution of the whispering gallery modes withing the fiber cavity, together with an estimation of the azimuthal and radial order modes. Thereafter, of 44h ion-exchanged WGM cavities were thermal poled showing that they exhibit different modal characteristics (Q-factors and appearance of modal families) when excitation was attempted for different azimuthal positions.

Lastly, we investigated the effects of the ion-exchange process on the photoelasticity of the borosilicate glass cavities by using the strain implemented technique which allows a direct measurement of the strain-induced birefringence, by monitoring spectral shifts of the WGMs resonances for TE and TM polarization. In parallel with hardness Knoop measurements using the micro-indentation method on typical BK-7 slabs that had gone through the same ion-exchange process, modifications of the Young's modulus were observed.

2 Experimental Processes and Apparatuses

2.1 Specifications of the borosilicate glass optical fiber

The specifications of the borosilicate glass optical fiber used in this experiment will be presented in this section; this specialty optical fiber is manufactured by Fiberoptics Technology inc., USA. The fiber has a total diameter of 78 μm, a guiding core of 71 μm in diameter and a Numerical Aperture of 0.66. The refractive index of the cladding layer was estimated to be 1.41(2) and by using the equation:

$$NA = \sqrt{{n_{core}}^2 - {n_{cladd}}^2} \tag{6}$$

the core's refractive index was estimated to be 1.56(2). The fibers were constantly cleaned with isopropanol throughout the experiment. A SEM cross-section of the fiber is shown in Figure 2.1.

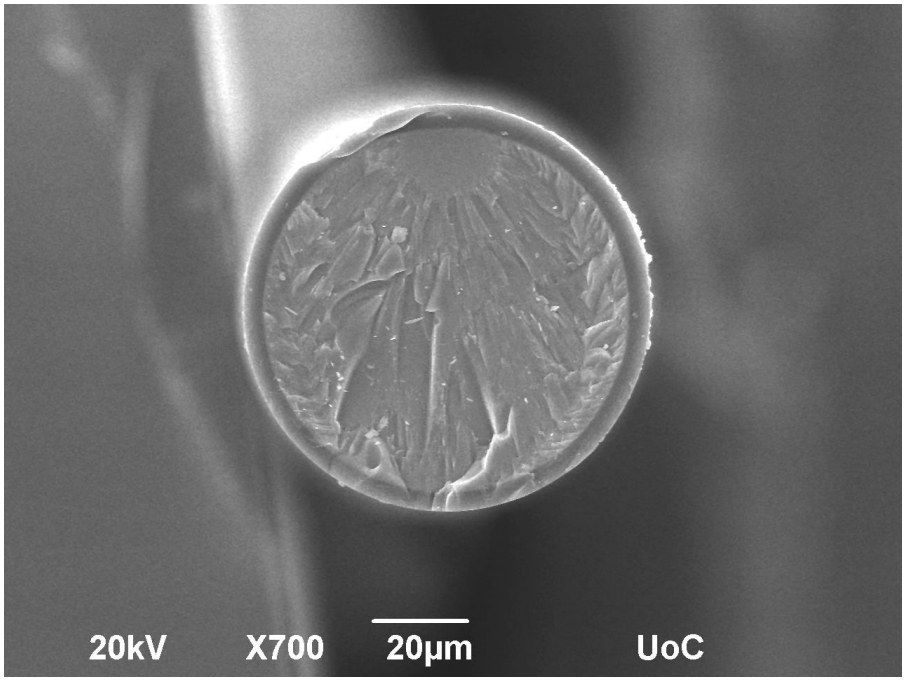

Figure 2.1: SEM picture of the cross-section of the borosilicate glass optical fiber. The fiber's core and cladding layer can be distinguished due to their large refractive index difference.

2.2 Ion Exchange process and apparatus

Borosilicate glass optical fibers were K^+ ion exchanged in a potassium nitrate melt, using typical procedures reported by José E. Roman [8]. Potassium nitrate (KNO_3) pellets with 99% purity provided by Honeywell research chemicals, was melted in a Pyrex glass tube at 395°C, which tube was placed inside an electrical vertical furnace. The borosilicate glass fibers were inserted in the Pyrex glass tube after the KNO_3 was a homogeneous melt. The ion-exchange process applied for typical times of 11, 22 and 44 hours. After the end of the ion-exchange process, the borosilicate glass fibers were removed before the solidification of the salt, using a pair of tweezers and they were cleaner using deionized water and then isopropanol.

2.3 Fabrication of Tapered Optical fibers

For the fabrication of the optical fiber taper (OFT), a single-mode optical fiber, standard telecom optical fiber SMF-28 was used and it was tapered to a diameter of 2.2 μm. The OFTs are fabricated by the heat and pull method, while using a dedicated commercial unit manufactured by Vytran® (GPX3000). With this process, the cladding and core of the initial fiber got thinner causing the light to be propagated within the cladding instead of the core. A photograph of the Vytran® OFT glass processing unit is shown in Figure 2.2.

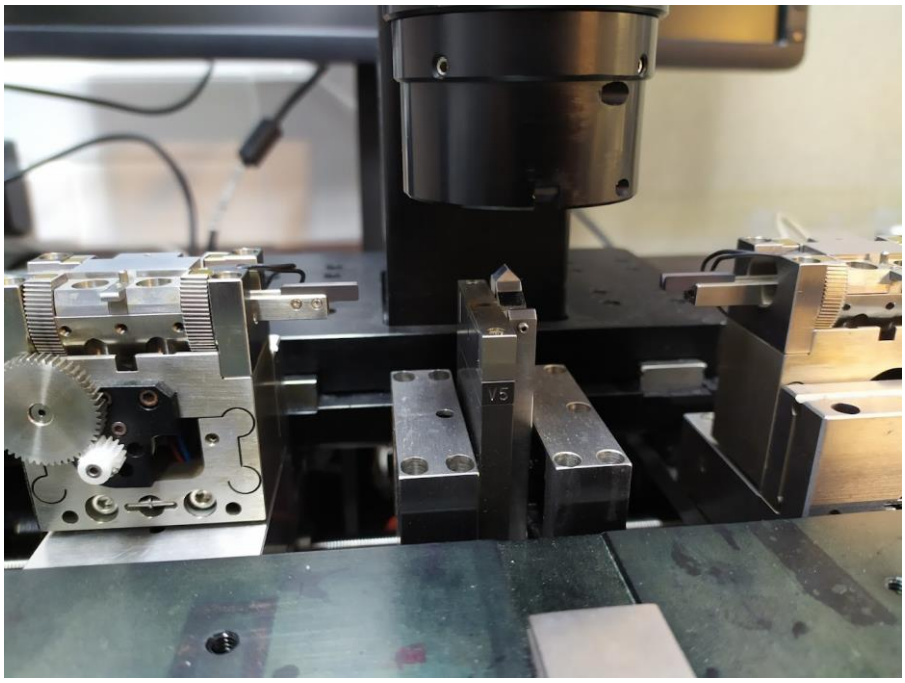

Figure 2.2: Photograph of the Vytran® OFT glass processing unit.

2.4 Spectral Characterization Apparatus for WGM cavities

A schematic representation of the experimental apparatus used for spectrally characterizing the whispering gallery mode resonation in the borosilicate glass optical fiber cavities, is shown in Figure 2.3.

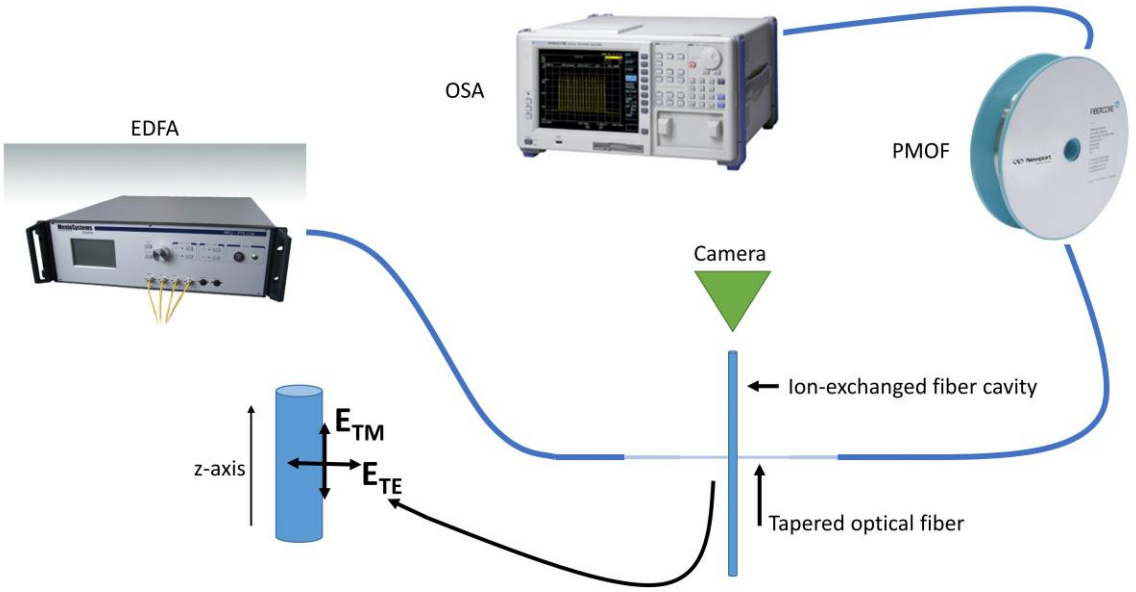

Figure 2.3 Schematic of WGM spectral characterization apparatus.

An erbium-doped fiber amplifier (EDFA) light source, emitting at the 1.5μm band, was used for exciting the WGM in the borosilicate glass cavity. An optical fiber taper (OFT) made from SMF-28 standard optical fiber, was used for exciting the WGMs in the cylindrical borosilicate glass optical cavities, while being placed in contact mode with the cavity outer surface. The OFT was tapered using the apparatus of section 2.3 and had a diameter of 2.2 μm. The output from the OFT was connected to a polarizing-maintaining optical fiber (PMOF), F-HB1550-11/125-Z, manufactured by Fibercore. The PMOF was 6 meters in length with a polarization extinction ratio of ≥ 30 dB. With the help of an optical fiber rotator, it was possible to choose between transverse electric (TE) and transverse magnetic (TM) polarization. The signal was received by an optical spectrum analyzer (OSA), AQ6317B, using 0.01 nm resolution. The camera was used to confirm the normal (vertical) positioning between the OFT and the WGM cylindrical resonator.

When the electric or magnetic component of the electromagnetic wave within the tapered fiber are perpendicular to the cavity's axis it is defined as transverse electric or transverse magnetic respectively (Fig. 2.3).

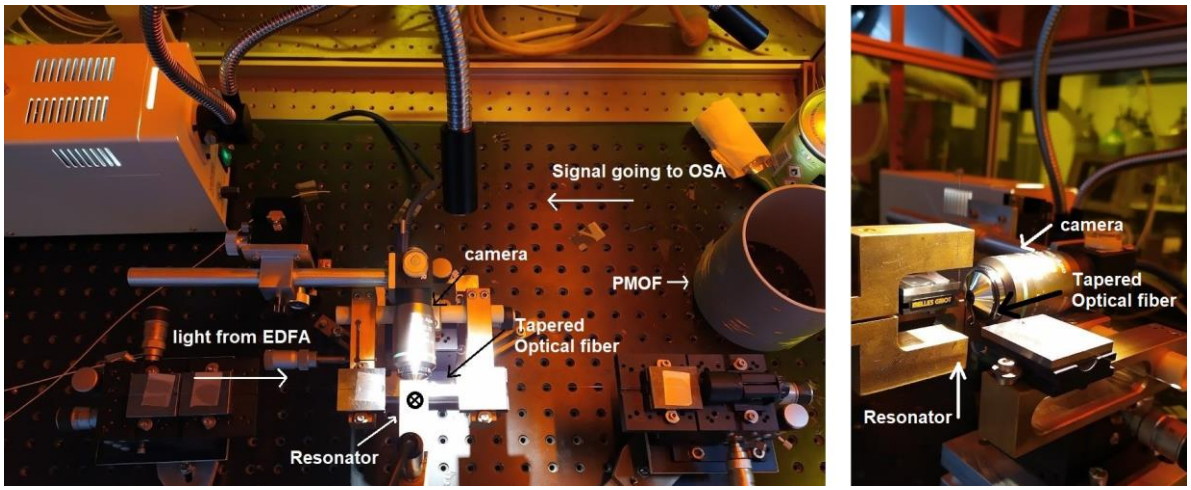

Figure 2.4: Photographs of WGM spectral characterization apparatus.

2.5 Apparatus used for application of strain to the borosilicate glass WGM cavities

The borosilicate glass WGM cavities were also spectrally characterized under the application of controlled longitudinal strain, for investigating their photo-elastic response. For doing so, a specialty made actuation fork was used (see Fig.2.5). The borosilicate glass optical fiber WGM cavity was firmly attached on the front side of the fork using Pattex epoxy glue with a resistance to traction up to 130 Kg/cm². Then, the borosilicate glass WGM cavity was slightly strained so to remove bending effects and light was coupled using the apparatus and process described in 2.4, for obtaining a reference measurement for TE and TM polarization states. Afterwards, longitudinal strain was applied in 2 μm steps using motorized actuator made by Thorlabs® with a 0.1 μm resolution step. After concluding a set of strain related measurements, the actuator was shifted back to its initial position so to measure backlash/hysteresis effects.

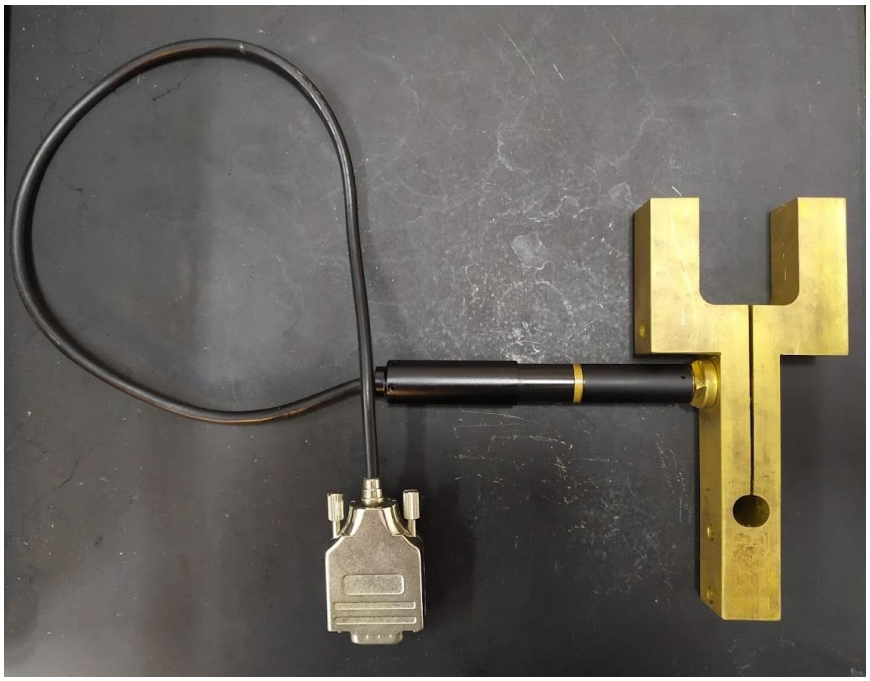

Figure 2.5: The metallic fork with the motorized actuator made by Thorlabs®.

2.6 Thermal poling Apparatus

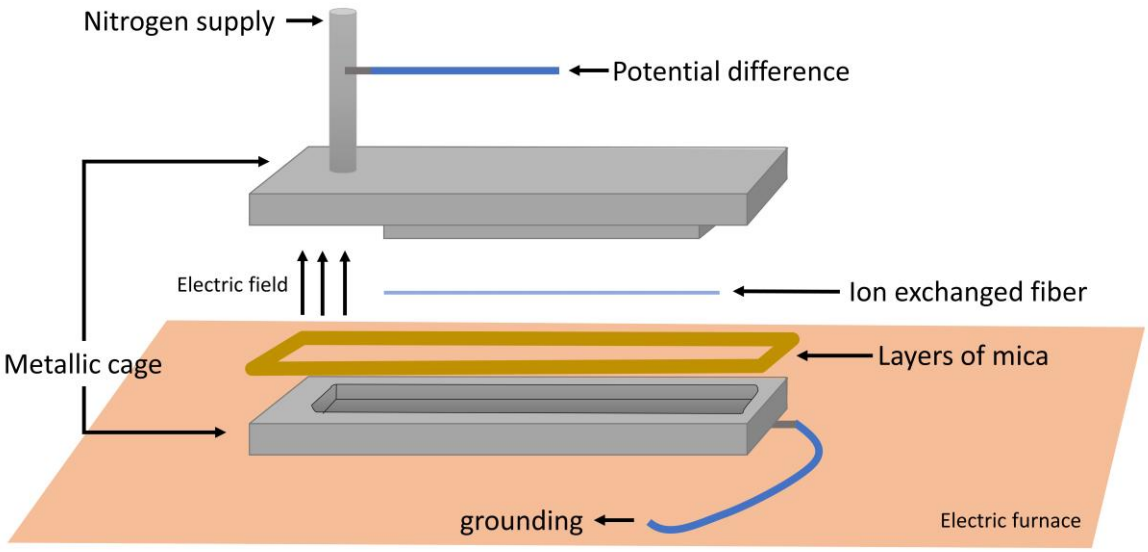

Figure 2.6: Poling Apparatus.

Borosilicate glass fibers that have been ion-exchanged for 44 hours were thermally poled. The apparatus used for thermal poling is presented in Fig. 2.6. The thermal poling chamber was a twofold structure, made from stainless steel, as non-conducting electrode configuration. A mica plate of 1.43 mm thickness was used to isolate the top and lower parts, operating as opposing polarity electrodes, with the positive pole connected at the lower part. The chamber had one gas input and suitable orifices for placing a thermocouple inside and for gas flow relaxation. During thermal poling process a nitrogen flow of 65 cm^3/sec was applied for avoiding hydroxyl impregnation into the poled glass matrix. All the stainless-steel chamber apparatus was placed on the top of a heating plate, with a controller for temperature stabilization of ± 1°C. As a result, the electric field was of perpendicular direction to the electrode plane. The electrode configuration applied resulted in a gap of 1 mm between the two polished, stainless-steel electrodes. A temperature of 250°C and a voltage difference of 1700V was applied during thermal poling. The duration of thermal poling was 60 min.

After the poling time was over, the heating plate was switched off with the high voltage being on, until the sample reaching room temperature.

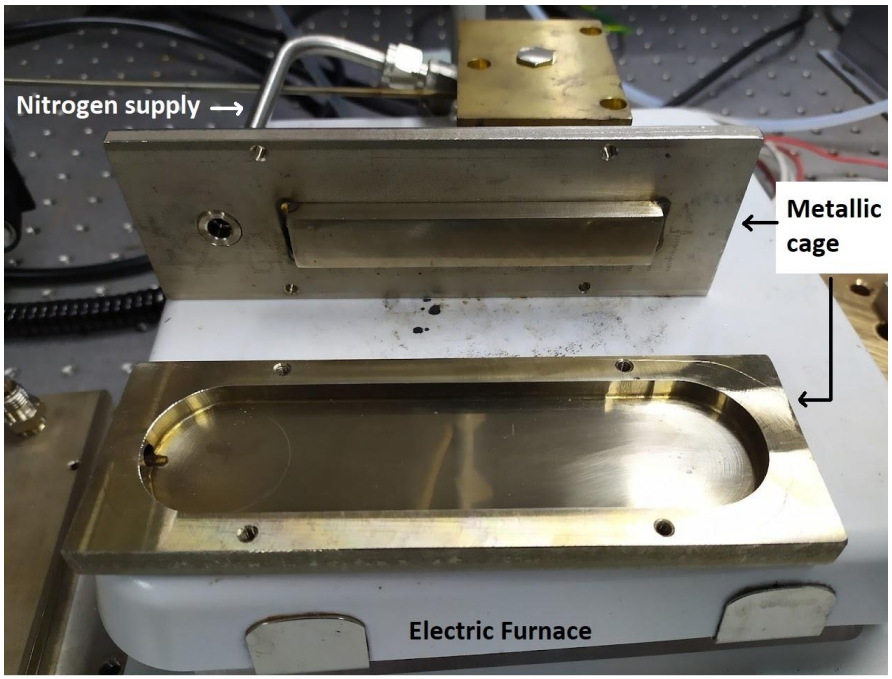

Figure 2.7: Photograph of the metallic cage.

3 WGMs in Ion Exchanged Borosilicate Glass Optical Fiber cavities

3.1 Introduction

In this section, the spectral characterization of the pristine and potassium ion-exchanged cylindrical, borosilicate glass WGM cavities will be presented. Upon studying the polarization-resolved spectra obtained for the two types of the WGM cavities, useful conclusions will be drawn about the impact of the ion-exchange process to the modal/resonating properties of those glass cavities.

3.2 Spectral characterization of pristine borosilicate glass WGM cavities

Initially, the spectral characterization of the pristine borosilicate glass cavities was carried out, while using the apparatus shown in 2.4. The cavities were attached on the front side of the specialty designed mounting fork using Pattex epoxy glue, and they were thoroughly strained so to remove bending effects. The optical signal was measured using an OSA, tuned at 0.01 nm resolution, for a wavelength range between 1540nm and 1560nm. Typical transmission spectra for TE and TM polarization states are presented in Fig.3.1. The Q-factor of those WGM resonances was measured to be $4.2 \cdot 10^5$ for TE and $5.9 \cdot 10^5$ for TM polarizations. From the refractive index data for the specific glass fiber provided by the manufacturing company and SEM cross-sectional pictures obtained for this optical fiber cavity, the azimuthal and polar modal order of the resonating notches were estimated, with corresponding free spectral range (FSR) between notches of the same azimuthal order to be FSR = 7.04 nm for both polarizations.

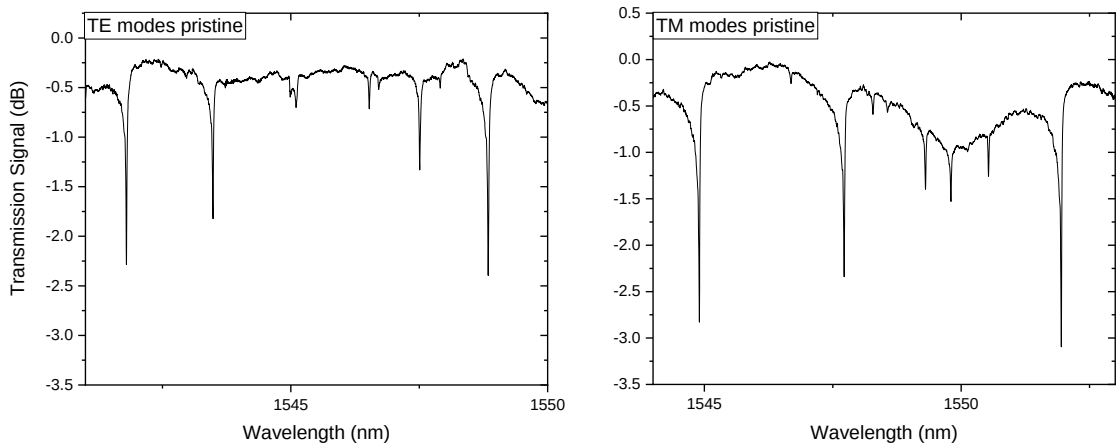

Figure 3.1: WGM spectra of pristine borosilicate glass WGM cavity for a) (left) transverse electric (TE) and b) (right) transverse magnetic (TM) polarization states.

3.3 Ion Exchanged cavities

Using the same experimental apparatus and measurement protocol, the transmission spectra for potassium ion-exchanged WGM cavities are presented in Fig 3.2. Ion-exchange times of 11h, 22h and 44h were applied for the samples examined.

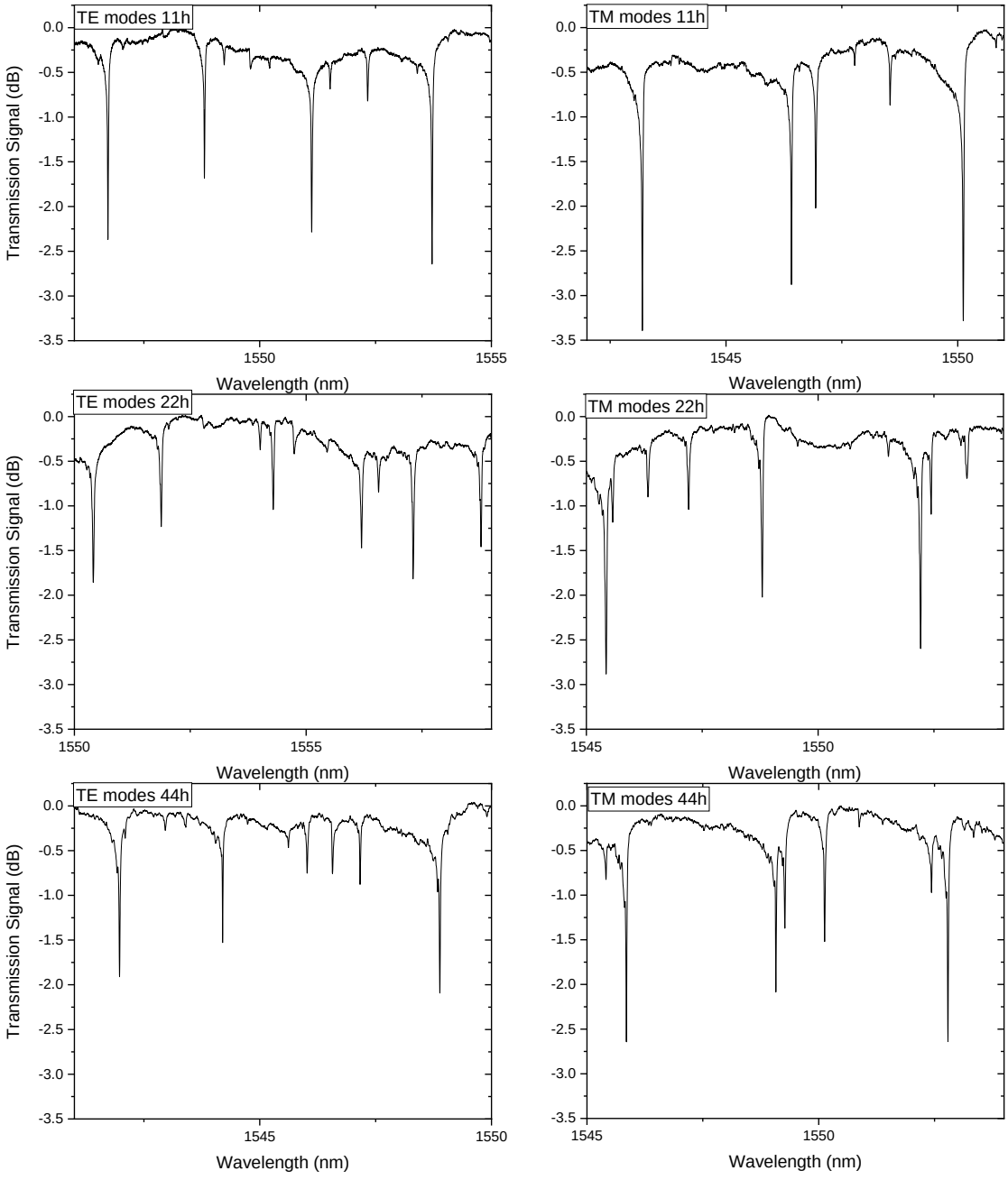

Figure 3.2: WGM spectra of ion exchanged borosilicate glass WGM cavity for TE and TM polarization states of a) (top) 11h, b) (middle) 22h and c) (bottom) 44 hours.

Measuring the FSRs from the WGM spectra and using the eq. 5, it is possible to calculate the refractive index of the cladding layer of the borosilicate glass fiber cavity, where the first radial order modes are located; accordingly, the refractive index change due to the ion exchange process while assuming that the 1st radial order modes are mostly confined in this outer layer. In the table, Fig. 3.3 below are shown the measured FSR and refractive indices depending on the ion exchange times.

		Pristine	11h	22h	44h
TE	FSR±0.01 (nm)	7.04	6.94	6.92	6.91
	n±0.004	1.411	1.431	1.435	1.437
	Δn±0.006	-	0.020	0.024	0.026
TM	FSR±0.01 (nm)	7.04	6.97	6.94	6.93
	n±0.004	1.411	1.425	1.431	1.433
	Δn±0.006	-	0.014	0.020	0.022

Figure 3.3: Table with FSR and refractive index changes in the borosilicate fiber glass after the potassium ion-exchange, depending on the ion-exchange times.

From the spectra of Fig.3.2, one can conclude that the ion-exchange process increases the refractive index of the borosilicate glass optical fiber cladding, allowing more efficient excitation of higher-order radial modes, as mostly appearing for the samples that have been ion-exchanged for 44h. Also, the data in Table 3.3 show that the prolongation of the ion-exchange process has little impact on the actual refractive index changes introduced into the borosilicate glass matrix, due to ion-shielding effects. Another important observation is related to the birefringence introduced into the borosilicate glass cavities after the potassium ion-exchange process; this is a typical finding related to the polarizability of the potassium ion and its coordination in the Na ion-exchange sites.

3.4 Results of Energy-dispersive X-ray spectroscopy

Using the energy-dispersive X-ray spectroscopy technique (EDX), the concentrations profiles of the potassium and sodium ions, along the transversal (radial) direction of the ion-exchanged cavities were obtained. The profiles come from a line parallel to the surface on a flat part of the cross-section at different depths.

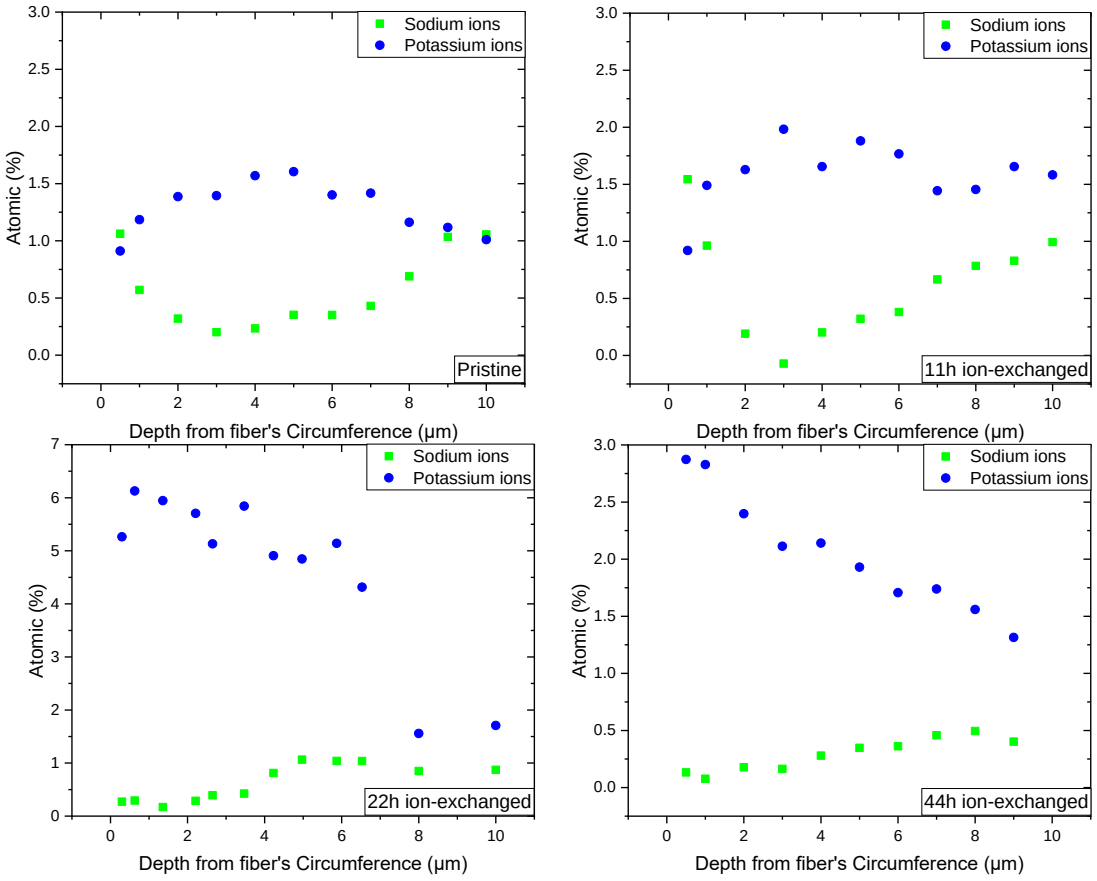

Figure 3.4: Potassium and sodium concentrations profiles of a) (top left) pristine, b) (top right) 11h, c) (bottom left) 22h and d) (bottom right) 44h ion exchanged cavities.

EDX measurements were employed so to obtain a first estimation of the ion-concentrations modified during the potassium ion-exchange process and correlate this with the refractive index profile of the processed optical fiber. From the data of Fig. 3.4 one can see that the potassium ion-concentrations have been substantially increased for the processed borosilicate glass optical fibers, augmenting the specific ion concentration by a factor of X2 for the sample ion-exchanged for 44h; corresponding Na-ion reductions are complementarily obtained for the same samples.

3.5 Simulations

Using the COMSOL Multiphysics package, simulations of the WGM cavities were performed so to obtain corresponding transmission spectra for the two polarization components. The initial variables of refractive indices and diameters were obtained from the experimental results presented in section 1.3. In these simulations, it is hypnotized that the refractive index changes are localized only in the cladding layer of the fiber cavity. The degrees of those changes are the ones measured in the actual WGM spectra.

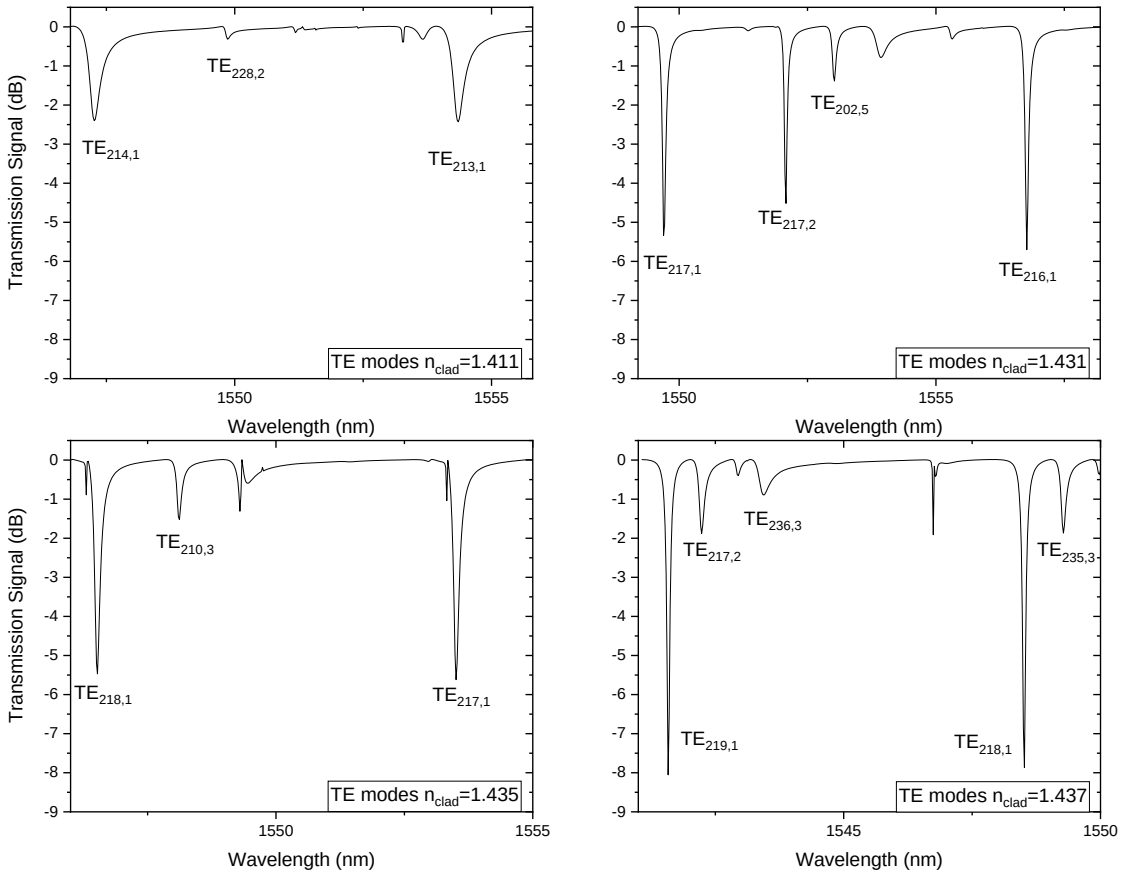

Figure 3.5: WGM spectra for TE polarization of simulations with an increasing refractive index of the cladding. The refractive index for the cladding layer is a) (top left) n=1.411, b) (top right) n=1.431, c) (bottom left) n=1.435 and d) (bottom right) n=1.437.

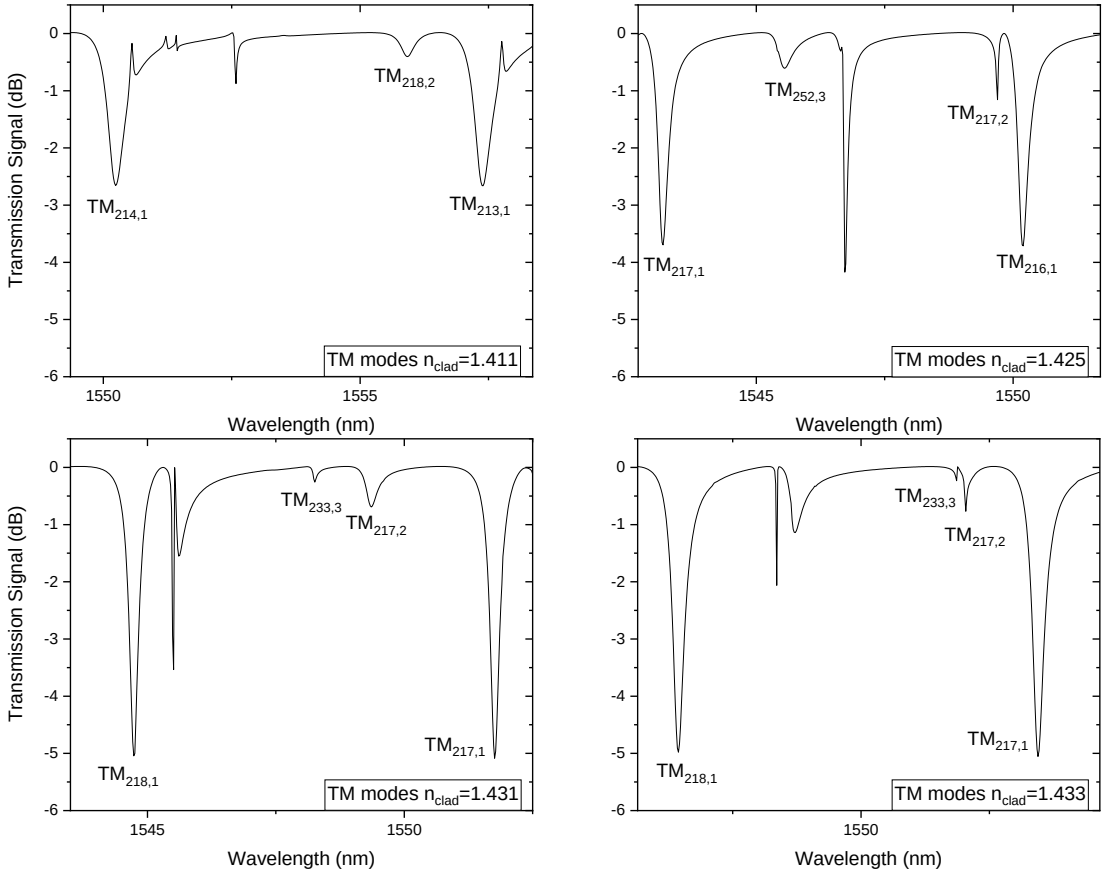

Figure 3.6: WGM spectra for TM polarization of simulations with an increasing refractive index of the cladding. The refractive index for the cladding layer is a) (top left) n=1.411, b) (top right) n=1.425, c) (bottom left) n=1.431 and d) (bottom right) n=1.433.

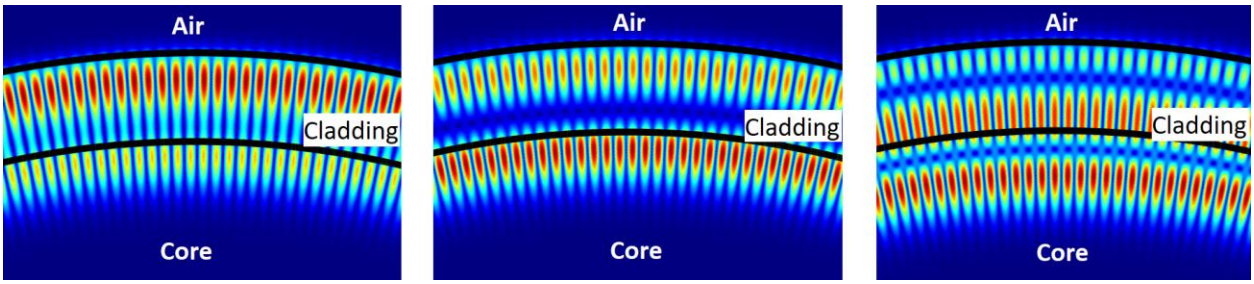

Figure 3.7: Images from simulations illustrating the first three whispering gallery radial modes, a) (left) first, b) (middle) second and c) (right) third radial mode

3.6 Discussion

The effects of ion exchange on the WGM spectra in borosilicate glass optical fibers are presented. The ion exchange process resulted in an increase in the refractive index of the exchanged layer of the cavity, depending on the ion-exchange time. This was the outcome of compressive stress due to the fact that the relevant radii are r_{Na^+}=0.095 nm and r_{K^+}=0.133 nm.

From the potassium and sodium concentrations profiles, it is shown a quantitative picture of the degree and depth of the ion exchange.

From the WGM spectra it is shown that with the increase of the ion exchange time and thus the increase of the refractive index, higher-order modes start to appear in the spectra. This is supported by the simulations and might be caused by the shortening of the refractive index step between the fiber's cladding and core.

4 WGMs of thermal poled ion-exchanged borosilicate glass optical fiber cavities

In this section we examine WGM resonation in thermally poled potassium ion-exchanged cylindrical, borosilicate glass fiber cavities. This step is done so to investigate the effect of non-symmetrical ion-migration and corresponding refractive index annular changes, in the spectral characteristics of the WGM resonances.

4.1 Experimental

Using the apparatus shown in 2.6, potassium ion-exchanged borosilicate glass cavities for 44-hour exchange time, were thermally poled. The duration of thermal poling was 60 min at a temperature of 250°C, while applying a voltage difference of 1700V and the spacing between the electrodes was 1mm. Afterward, WGMs spectra for both polarizations were measured per 15° around the cavity's circumference.

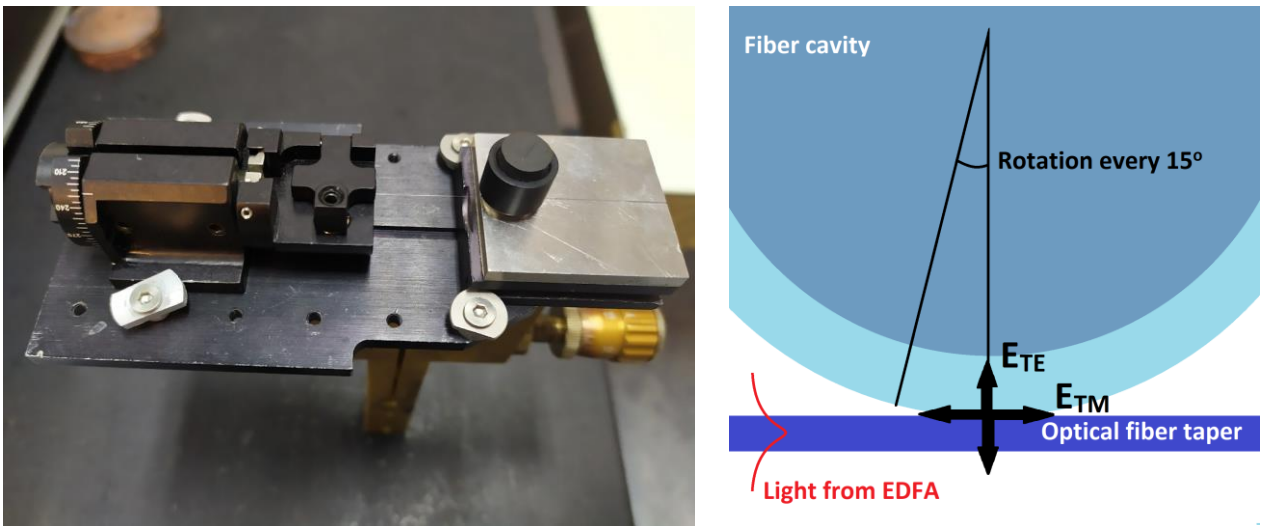

Figure 4.1: (Left) Photograph of poled ion-exchanged fiber on an optical fiber rotator that allows freely and precise rotations. (Right) Schematic of the coupling between the poled fiber cavity and the optical tapered fiber.

4.2 WGM spectra of poled ion-exchanged cavity

The WGM spectra of thermally poled, potassium ion-exchanged cylindrical, borosilicate glass fiber cavities for TE and TM polarizations, per 90° around the cavity's circumference, are presented in the figures 4.1 and 4.2. The spectra are illustrating two consecutive FSRs.

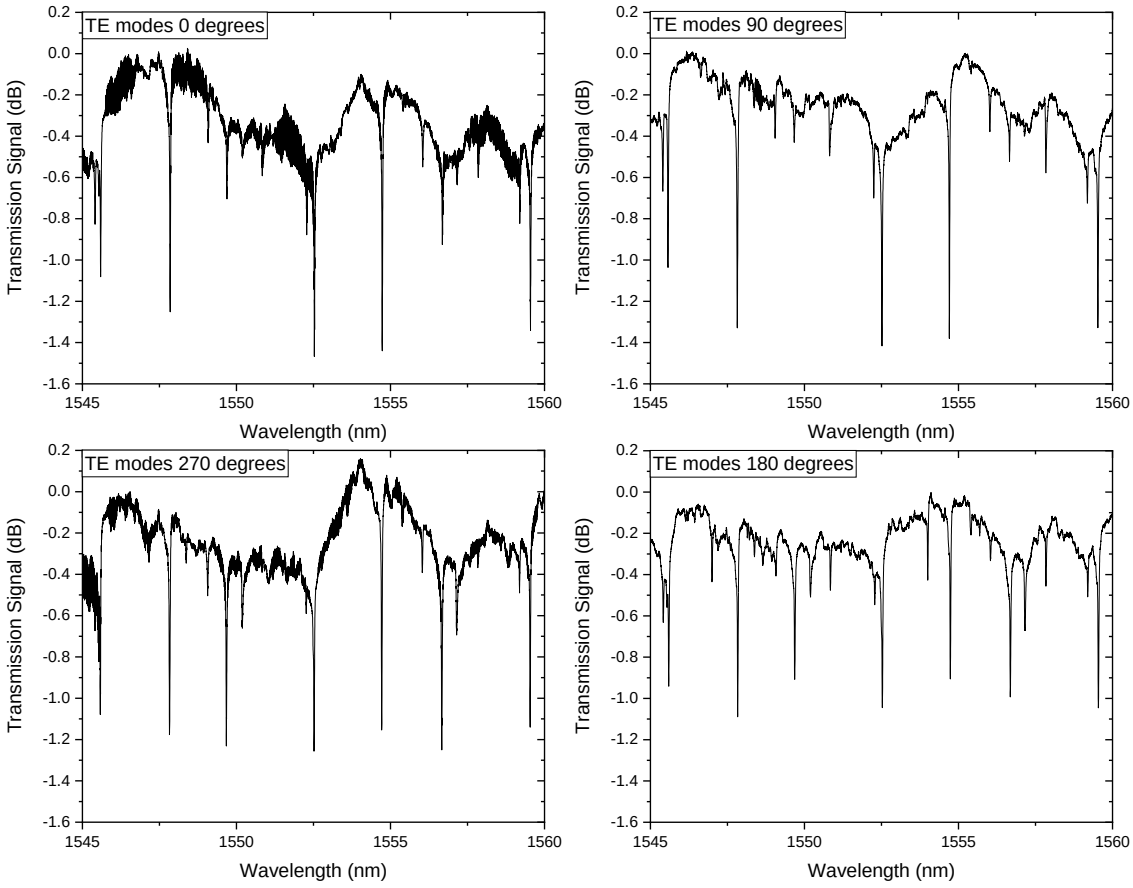

Figure 4.1: WGM spectra for thermal poled ion-exchanged cavities for TE polarization. The spectra are taken for different angles around the cavity's circumference: a) (top left) 0°, b) (top right) 90°, c) (bottom left) 270° and d) (bottom right) 180°.

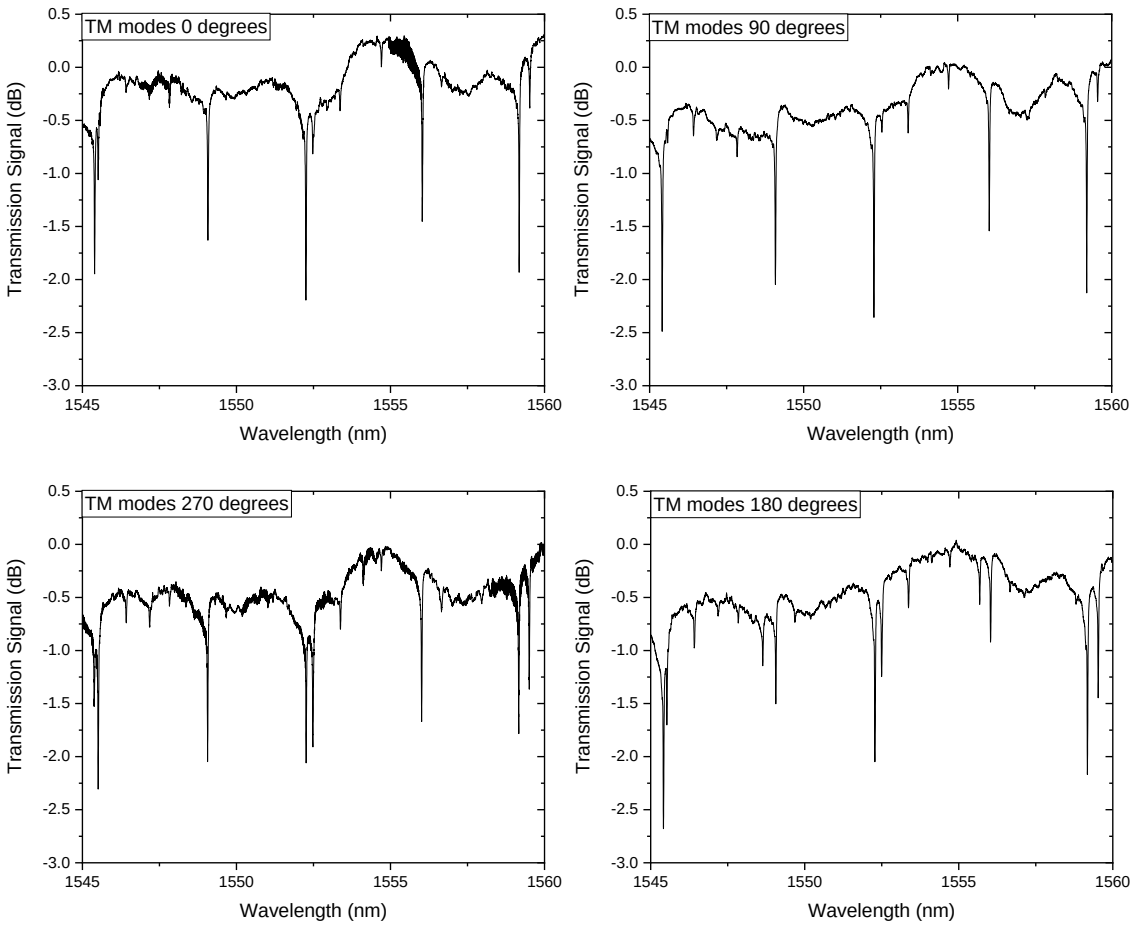

Figure 4.2: WGM spectra for thermal poled ion-exchanged cavities for TM polarization. The spectra are taken for different angles around the cavity's circumference: a) (top left) 0°, b) (top right) 90°, c) (bottom left) 270° and d) (bottom right) 180°.

4.3 Refractive index and Q factor changes

From the interpretation of the WGMs spectra, near surface refractive index values and Q factor were calculated, for different angular WGM excitations performed around the cavity's circumference. Figure 4.3 illustrates refractive index changes around the cavity for both polarizations; accordingly figure 4.4 include Q factor for the same mode while being excited for different angular positions of the glass cavity with respect to the optical fiber taper.

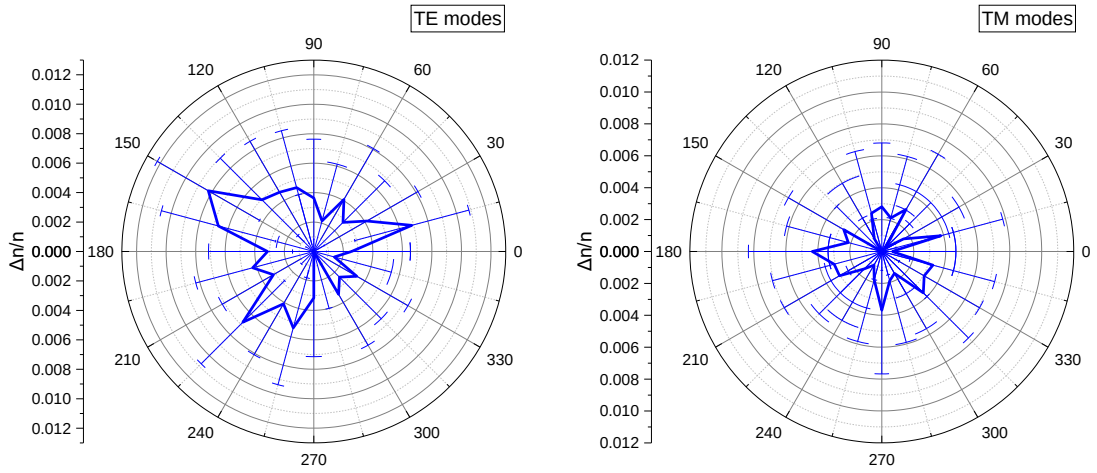

Figure 4.3: Graph of refractive index changes around the thermal poled ion-exchanged cavity's circumference for TE and TM polarization.

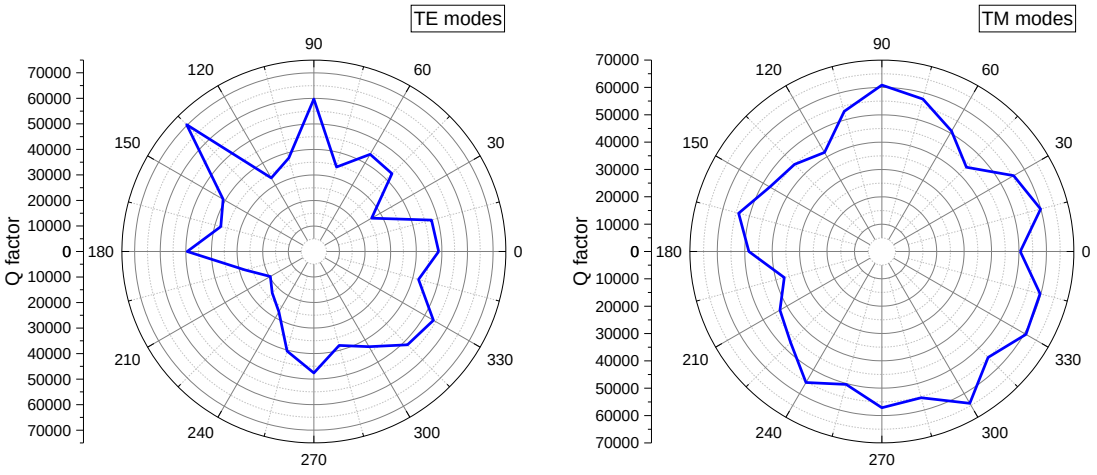

Figure 4.4: Graph of Q factor changes around the thermal poled ion-exchanged cavity for TE and TM polarization. The error bars were too small to be illustrated.

4.4 Discussion

Borosilicate glass optical fiber cavities that were 44 hours potassium ion-exchanged were thermally poled, and afterwards their WGMs spectra were obtained for different angular points from around the cavity's circumference. The application of thermal poling transversally to the optical fiber axis, will break the symmetry of the refractive index of the borosilicate glass optical fiber cavity. Such a type of angularly oriented refractive index perturbation, will facilitate different modal excitation conditions for the same cavity with respect to the azimuthal positioning of the cavity with respect to the optical fiber taper. Differential excitation will predominantly affect the Q-factor of modes excited and the appearance/suppression of modes that are of lower overlap with the evanescence field of the optical fiber taper.

The WGMs spectra of Figures 4.1 and 4.2 show an increase in the extinction ratio of higher-order radial modes near 180° ±30°, holding for both polarizations. This is in good agreement with the increase of the refractive index observed for the same range of angles (see Fig. 4.3), allowing the higher order radial modes shifting towards the outer surface of the borosilicate glass cavity. This phenomenon, a higher refractive index leading to the appearance of higher-order modes, was also noticed in section 3.2 with the ion-exchanged cavities. Further examination of the resonating characteristics of the thermally poled, potassium ion-exchanged cylindrical, borosilicate glass fiber cavities is not within the scope of this thesis.

5 Strain application on ion-exchanged borosilicate glass optical fibers WGMs cavities

5.1 Introduction

In this section, the photoelastic behavior of the potassium (K^+) ion-exchanged, borosilicate glass, optical fiber cavities under the application of axial strain were studied. This strain implemented technique allows a direct measurement of the strain-induced birefringence and the determination of the Pockels' coefficients by means of the spectral shift of the WGMs resonances for TE and TM polarization[9], [10].

For fully elaborating the experimental data and understanding the underlying impact of the ion-exchange process on to photoelasticity of the borosilicate glass cavities, the elastic modulus to hardness ratio was determined using Knoop indentation measurements on ion-exchanged BK-7 borosilicate glass wafers. The last allowed the determination of the modification of Young's modulus of the ion-exchanged glass as a function of the ion-exchange time.

5.2 WGMs spectra characterization of ion-exchanged cavities

The potassium ion-exchanged borosilicate glass, optical fiber whispering gallery mode cavities were spectrally characterized using the setup and procedure, presented in 2.4. Using the apparatus shown in section 2.5, controlled longitudinal strain was applied in 2 μm steps using motorized actuator made by Thorlabs® with a 0.1 μm resolution step. At the end of each set of measurements, the actuator was shifted back to its initial position so to measure backlash/hysteresis effects. The wavelength shifts of the WGM resonances in 11-, 22- and 44-hours ion-exchanged, borosilicate glass, optical fiber whispering gallery mode cavities as a function of strain was measured for both TE and TM polarizations.

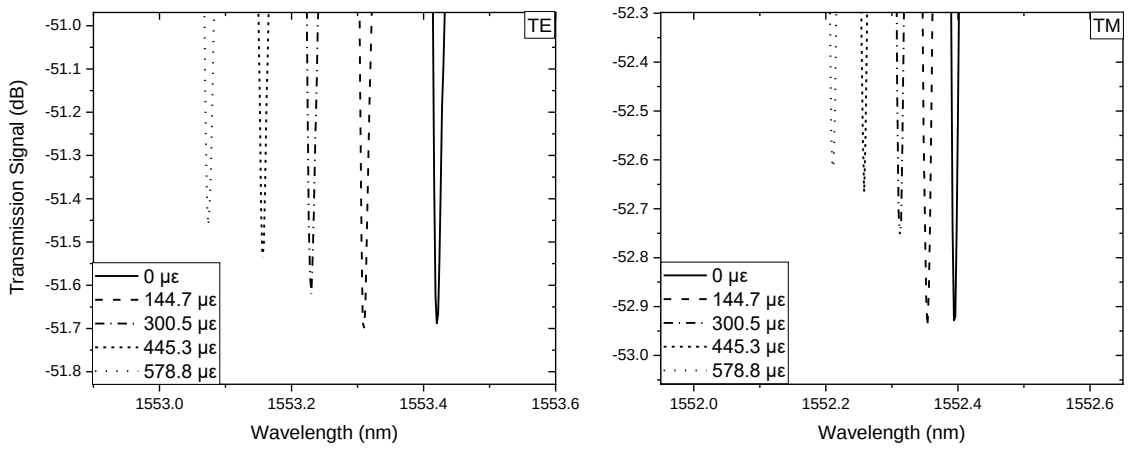

Figure 5.1: Blueshifts of resonance wavelength for the a) (left) TE and b) (right) TM polarizations with increasing applied strain ε.

Selectively, the relevant blueshifts of the WGMs resonances due to the applied strain, for (a) TE and (b) TM polarizations are illustrated in Fig. 5.1. The anisotropy between the two polarizations is revealed distinctly as the blueshifts for the TM modes are lower compared to those of TE.

Measuring the blueshift of resonance wavelength of potassium ion-exchanged borosilicate glass, optical fiber whispering gallery mode cavities, graphs with relative wavelength shift as a function of strain can be produced. In Fig. 5.2 is shown the slopes of the linear regressions that fit the experimental values for each ion-exchange time.

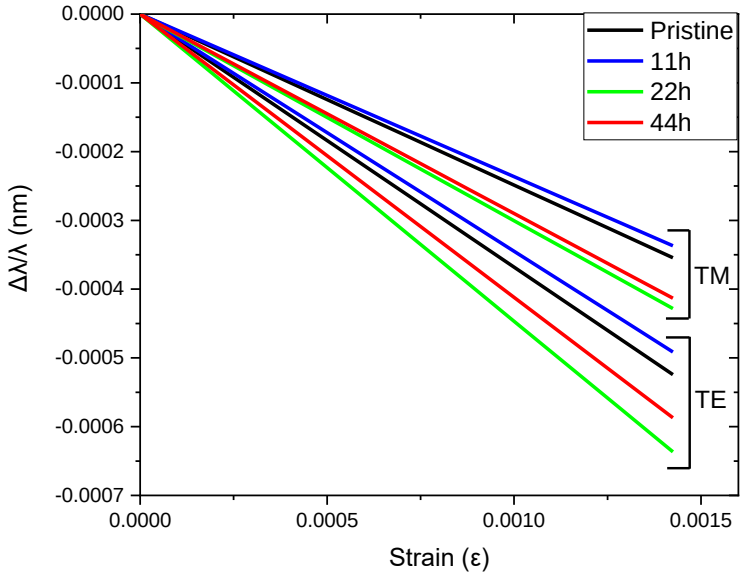

Figure 5.2: Relative wavelength shift of TE- and TM-polarized WGM resonances as a function of strain for pristine and ion-exchanged cavities.

The changes of the strain induced birefringence (TE-TM)/ε slope values (ζ) evaluated from the data of Fig.5.2 as a function of the potassium ion-exchange time are shown in Fig. 5.3. It is observed that for the first 11 hours of potassium ion-exchange there is a small increase followed by a noticeable descent for higher ion-exchange times. The changes observed in the strain induced birefringence for borosilicate glass fiber samples subjected to different ion-exchange times, are attributed to three distinct parameters: molar refractivity changes, subsequent modal profile changes for the whispering gallery modes, and changes in the mechanical properties (Young modulus and Poisson ratio) of the glass fibers. The strain induced birefringence slope values (ζ) estimated here together with the Young's moduli data found from the hardness Knoop test following, will used for the determination of the Pockels' elasto-optic coefficients for the pristine and ion-exchanged borosilicate glass cavities.

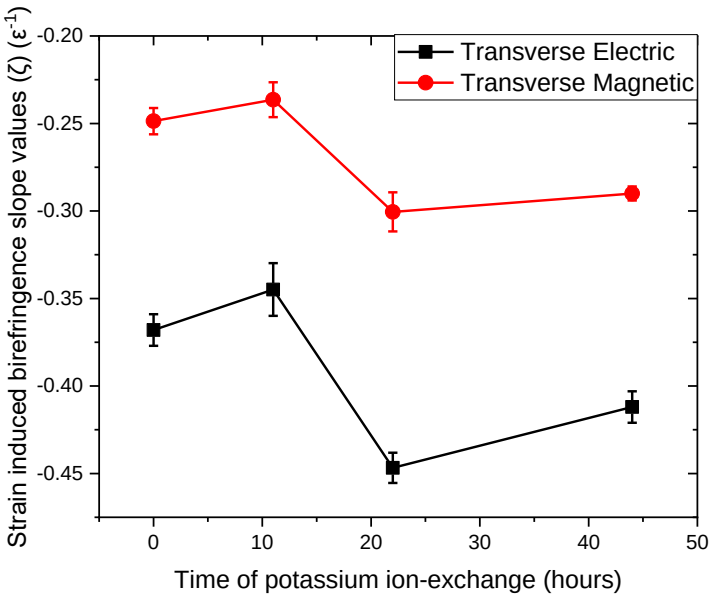

Figure 5.3: Strain induced birefringence (TE-TM)/ε slope values (ζ) for TE- and TM-polarization states as function of the potassium ion-exchange time.

5.3 Hardness Knoop

The cylindrical geometry of the borosilicate glass, optical fibers used in ion-exchanged constitutes a major obstacle for directly measuring their mechanical properties (Young's modulus) using available micro-indentation methods. Instead, for gaining basic insights into the role of potassium ion-exchange in the resulting modifications of Knoop hardness of borosilicate glass, we decided to employ micro-indentation measurements in typical BK-7 slabs using the same ion-exchange conditions, applied in the optical fiber whispering gallery mode cavities. Such a type of study will allow us trace the actual differences in the Young's modulus introduced by the diffusion of the potassium ions and the replacement of the corresponding sodium ions.

For estimating changes in the Young's modulus of borosilicate glass, the method of Marshall, et al [11] was employed, where the young modulus of a material is deduced by the elastic recovery of the in-surface dimensions of a Knoop hardness indentation. The indentation experiments were conducted using a Universal indentation hardness tester apparatus (LM series). The indentations were performed by applying a 200-gr weight on commercial BK-7 (UQG, UK) borosilicate glass slabs that have been ion-exchanged with the same apparatus and conditions used for the optical fiber cavities. The dimensions of the indentation imprints were measured using an optical microscope, with a 40x objective, with 0.2 μm resolution and electronic vernier eyepiece. Each measurement contained 15 indentation imprints dispersed over a large area of the BK-7 glass slabs; typical indentation imprints are shown in Fig. 5.4.

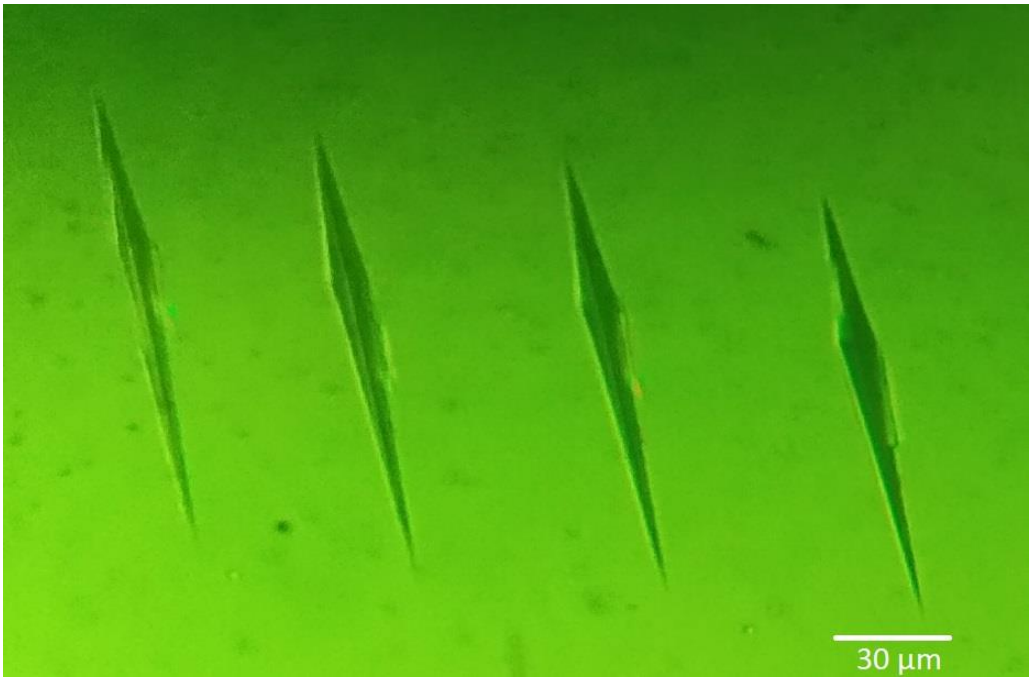

Figure 5.4: Photograph of Knoop indentations by a 200-gr weight on BK7 borosilicate glass ion-exchanged slab.

Measuring the dimensions of the indentations and in conjunction with the Marshall method, the hardness Knoop and later from that the Young's modulus were estimated as a function of the ion-exchange time.

$$\frac{b'}{a'} \approx \frac{b'}{a} = \frac{b}{a} - \boldsymbol{\alpha}\frac{H}{E} \tag{6}$$

where a and b the dimensions of the Knoop hardness test indenter, a' and b' the dimensions of the indentation, **α** experimental constant estimated to be 0.45, H the hardness and E the Young's modulus.

In Fig. 5.5 the behavior of those values is demonstrated. The hardness Knoop follows a steady increase as the ion-exchange time progresses. On the other hand, the Young's modulus in the early stages of the process, increases until around the 11 hours where suddenly it is reduced by 25 GPa at 22 hours of ion-exchange before returning back to its rising course. It should be mentioned that the determination of the Young's modulus using this method is quite sensitive to small changes in the dimensions of the indentations because it is calculated based on the ratio $\frac{b\prime}{a\prime}$.

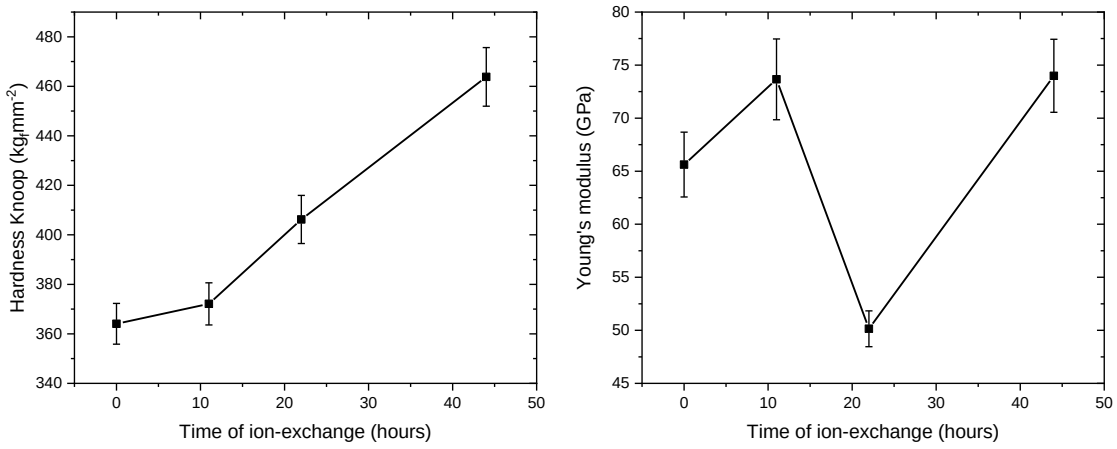

Figure 5.5: a) (left) Hardness Knoop and b) (right) Young's modulus depending on the ion-exchange time, estimated by using Knoop indentations on borosilicate glass wafers.

Finally, using the equations for the elasto-optic coefficients shown in 1.6,

$$\begin{aligned} \Delta B_x &= E_z p_{12} - (p_{11} + p_{12}) v E_z \\ \Delta B_x &= (p_{12} - (p_{11} + p_{12}) v) E_z \end{aligned} \tag{7}$$

and assuming that the Poisson's ratio ($v = 0.2$ for borosilicate glass) remains the same throughout the duration of the experiment, it is possible to estimate the coefficients p_{11} and p_{12},

which are shown in Fig. 5.6. What is observed is that the elasto-optic coefficients strongly imitate the behavior of the slope values of the TE- and TM-polarization states in reverse.

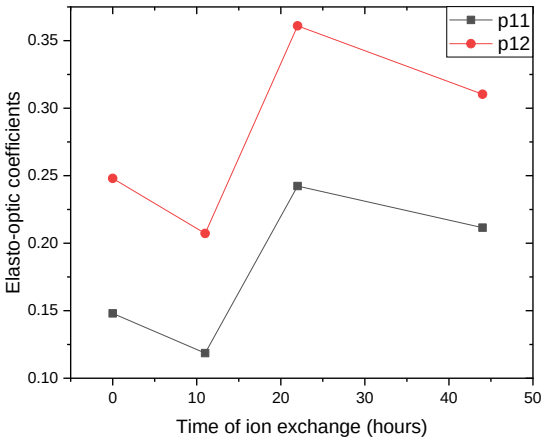

Ion-exchange time	pristine	11 hours	22 hours	44 hours
p_{11}	0.1480	0.1186	0.2423	0.2115
p_{12}	0.2480	0.2072	0.3610	0.3103

Figure 5.6: a) (left) Graph with the elasto-optic coefficient changes depending on the ion-exchange time and b) (right) table with the elasto-optic coefficient values.

5.4 Discussion

The effects of ion-exchange on hardness, Young's modulus and lastly on the elasto-optic coefficients of borosilicate glass optical fiber cavities were studied. This knowledge will help get a better understanding of the processes that take place inside the glass during the ion-exchange treatment using a melt bath of KNO_3.

By applying longitudinal strain to an isotropic cylindrical microresonator and measuring the blueshifts of the resonance wavelength for pristine and ion-exchanged cavities it is possible to get a direct characterization of the uniaxial anisotropy of the elasto-optic effect. These measurements along with the Young's modulus obtained by the hardness Knoop test, enable the determination of the Pockels' coefficients for different ion-exchange times. Using this technique, the elasto-optic coefficients refer to the cladding material since the WGMs are surface waves guided by the outer interface of the optical fiber.

In Fig. 5.3 which shows the slope values for TE- and TM-polarization states and later again in Fig. 5.5b which shows the Young's modulus, both depending on the ion-exchange time, it is noticed as nonlinear behavior. This is happening because the exchange of K^+ ions gives rise to two competing processes, the generation of stress from foreign ions into small host ion sites in the glass, and the relaxation of stress using viscous flow. This is supported by previous studies [12] where it is reported that borosilicate glass strengthened by chemical KNO_3 bath has a maximum strength at 15 hours of treatment; when the ion-exchange process is saturated.

6 Conclusion

An analysis on the potassium (K^+) ion-exchange process in borosilicate glass, optical fiber whispering gallery mode cavities and the relevant mode shifting effects emerge, as well as the impact of ion-exchange process on the photoelastic properties of the glass cavity material have been examined in this thesis.

Optical fibers include a core surrounded by a cladding material with a lower index of refraction. The ion-exchange process of the borosilicate glass, optical fiber whispering gallery mode cavities led to an increase of the outer refractive index, assumed to be confined mostly in the thin cladding layer. The increase of refractive index of the thin cladding layer of these borosilicate glass fibers with potassium ion-exchange, results in enhancement of the excitation of the fundamental (1^{st}) radial order modes, also of the appearance of higher order radial modes; these effects are clearly manifested in the resonation spectra of those WGM cavities when excited using optical fiber tapers in evanescent fiend proximity mode. A detailed study of the Q-factors and the FSR values of the ion-exchanged WGM, borosilicate glass cavities is presented, while correlating the modal data obtained with EDX ion measurements of the potassium ions, so to gain basic insight on the yield of the ion-exchange process. Maximum refractive index changes after the potassium ion-exchange, being measured using WGM spectra, are of the order of 0.026 for a 44 hours ion-exchange time.

Then, thermal poling of potassium ion-exchanged borosilicate glass, optical fiber whispering gallery mode cavities was carried out, in an attempt to further control the modal characteristics of these ion-exchanged cavities. These results indicated that the thermally poled, ion-exchanged cavities exhibit different modal characteristics (Q-factors and appearance of modal families) when excitation was attempted for different azimuthal positions, with respect to the longitudinal axis of the cavity. This is clearly attributed to the asymmetrical refractive index profile, introduced by the thermal-poling process, primarily affecting the modal excitation characteristics by the optical fiber taper.

The impact of the ion-exchange process on the photoelasticity of the borosilicate glass cavities was investigated by using the strain implemented technique which allows a direct measurement of the strain-induced birefringence, by monitoring spectral shifts of the WGMs resonances for TE and TM polarization. The Pockels' coefficients of the ion-exchanged borosilicate glass were estimated from such strain facilitated WGM measurements, as a function of the ion-exchange time.

We expect that ion-exchange process can be used for further tuning the resonation characteristics of soft-glass cavities, also, being exploited in the realization of micro-lasing units and refractive index sensing probes. Further, investigations are necessary in order to consolidate the findings of this thesis, especially for the case of thermally poled WGM ion-exchanged cavities.

6.1 References

[1] Lord Rayleigh, "CXII. The problem of the whispering gallery," *The London, Edinburgh, and Dublin Philosophical Magazine and Journal of Science*, vol. 20, no. 120, pp. 1001–1004, Dec. 1910, doi: 10.1080/14786441008636993.

[2] J. W. S. Rayleigh, *The theory of sound*. London: Macmillan and Co., 1877.

[3] P. Debye, "Der Lichtdruck auf Kugeln von beliebigem Material," *Ann Phys*, vol. 335, no. 11, pp. 57–136, 1909, doi: https://doi.org/10.1002/andp.19093351103.

[4] G. Mie, "Beiträge zur Optik trüber Medien, speziell kolloidaler Metallösungen," *Ann Phys*, vol. 330, no. 3, pp. 377–445, Jan. 1908, doi: 10.1002/andp.19083300302.

[5] M. Noto, D. Keng, I. Teraoka, and S. Arnold, "Detection of Protein Orientation on the Silica Microsphere Surface Using Transverse Electric/Transverse Magnetic Whispering Gallery Modes," *Biophys J*, vol. 92, no. 12, pp. 4466–4472, 2007, doi: https://doi.org/10.1529/biophysj.106.103200.

[6] M. Cai, O. Painter, K. J. Vahala, and P. C. Sercel, "Fiber-coupled microsphere laser," *Opt Lett*, vol. 25, no. 19, p. 1430, Oct. 2000, doi: 10.1364/OL.25.001430.

[7] W. von Klitzing, R. Long, V. S. Ilchenko, J. Hare, and V. Lefèvre-Seguin, "Frequency tuning of the whispering-gallery modes of silica microspheres for cavity quantum electrodynamics and spectroscopy," *Opt Lett*, vol. 26, no. 3, p. 166, Feb. 2001, doi: 10.1364/OL.26.000166.

[8] P. Camy, J. E. Roman, M. Hempstead, P. Laborde, and C. Lerminiaux, "Ion-Exchanged Waveguide Amplifier in Erbium-Doped Glass for Broad-band Communications," in *Optical Amplifiers and Their Applications*, 1995, p. FD2. doi: 10.1364/OAA.1995.FD2.

[9] K. Milenko, S. Pissadakis, G. Gkantzounis, A. Aluculesei, and G. Fytas, "Probing Stress-Induced Optical Birefringence of Glassy Polymers by Whispering Gallery Modes Light Localization," *ACS Omega*, vol. 2, no. 12, pp. 9127–9135, Dec. 2017, doi: 10.1021/acsomega.7b01409.

[10] X. Roselló-Mechó, M. Delgado-Pinar, A. Díez, and M. v. Andrés, "Measurement of Pockels' coefficients and demonstration of the anisotropy of the elasto-optic effect in optical fibers under axial strain," *Opt Lett*, vol. 41, no. 13, p. 2934, Jul. 2016, doi: 10.1364/ol.41.002934.

[11] D. B. Marshall, T. Noma, and A. G. Evans, "A Simple Method for Determining Elastic-Modulus–to-Hardness Ratios using Knoop Indentation Measurements," *Journal of the American Ceramic Society*, vol. 65, no. 10, pp. c175–c176, 1982, doi: https://doi.org/10.1111/j.1151-2916.1982.tb10357.x.

[12] N. Bouras, M. A. Madjoubi, M. Kolli, S. Benterki, and M. Hamidouche, "Thermal and mechanical characterization of borosilicate glass," *Phys Procedia*, vol. 2, no. 3, pp. 1135–1140, Nov. 2009, doi: 10.1016/j.phpro.2009.11.074.